Investigation of Open-Winding PMSG System With the Integration of Fully Controlled and Uncontrolled Converter

Heng Nian, *Member, IEEE*, and Yijie Zhou

***Abstract*—An open-winding permanent-magnet synchronous generator (PMSG) system with the integration of fully controlled and uncontrolled converter is investigated in this paper, in which half the amount of controllable power switches are needed compared with the conventional open winding system fed by two voltage source converters. The voltage space vector of open winding PMSG is modulated by controlled converter, which will be integrated with the voltage vector by uncontrolled converter to implement the operation of open winding PMSG. In order to analyze and compare the operation capability on the different dc voltage ratios, the available modulation range of the open winding PMSG is analyzed in detail. Moreover, unity power factor control is proposed as the optimized control method to achieve the maximum modulation index. Finally, a 1-kW experimental setup is built to validate the theoretical investigation on the open winding PMSG system.**

***Index Terms*—DC voltage ratio, integration of fully controlled and uncontrolled converter, linear modulation range, open winding permanent-magnet synchronous generator (PMSG), unity power factor control.**

I. Introduction

THE permanent-magnet synchronous generator (PMSG) has been widely applied in various power conversion systems due to the high power density, flexible magnet topologies, and excellent operation performance [1]–[3]. As the power capacity and the voltage level of PMSG system increase, the full power rating converter for PMSG system places the higher requirements on the switch devices [4]. The open winding configuration for PMSG is proposed as a novel solution for the high power capacity of PMSG system by connecting the ac side of the generator with two voltage source converters (VSCs). Thus, many advantages, such as lower dc-link voltage, flexible control objective, and multilevel modulation effect can be achieved [5]–[13].

The traditional open winding PMSG system is shown in Fig. 1, in which the reduced capacity for one converter can be obtained. Up to now, many types of converter configurations have been proposed for the open winding power conversion system to synthesize a higher voltage level output [14]–[19]. In [20], the unity power factor control, voltage quadrature control, and optimum inverter control with open winding configuration were analyzed in detail and validated by experimental results. Nevertheless, if power rating of PMSG is fixed, the total VA rating of switch devices for the traditional open winding configuration is still the same as the star or delta-connected conventional PMSG system. Meanwhile, the amount of switch devices for the open winding PMSG system would be double due to employing two VSCs, which makes the system more complicated and jeopardizes the system reliability.

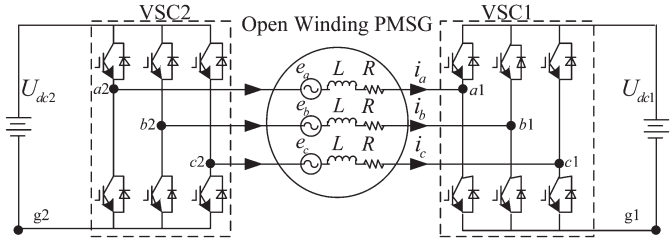

Fig. 1. Traditional open-winding PMSG configuration.

In order to reduce the total power rating of the all switch devices, an open winding power conversion system fed by two half-controlled converters (HCC) was proposed in [21]. Although the HCCs can guarantee immunity to dc bus shoot through, the calculation process for switching signal is complex. Furthermore, a series compensated open-winding-PMSG-based generation system was proposed in [22], in which the open winding PMSG is connected with a diode bridge and a VSC in each side of the stator winding. A capacitor is linked to the dc side of the VSC to compensate the active power output. Nevertheless, since the current on the diode bridge is not controllable and the corresponding control scheme is still conventional, the harmonic components of stator current are too high to limit the application in the high-power-conversion system. Thus, the operation mechanism and the optimized control strategy of the open winding PMSG system with single-side controllable VSC is still needed to be investigated.

In this paper, an open winding PMSG system with the integration of fully controlled and uncontrolled converter was investigated. Section II gives a brief introduction of the open winding PMSG system and tabulates a comparison of the proposed topology and other converters on the total switch

Manuscript received February 4, 2014; revised April 24, 2014 and June 4, 2014; accepted June 10, 2014. Date of publication June 18, 2014; date of current version January 16, 2015. Paper 2014-IPCC-0044.R2, presented at 2013 IEEE Energy Conversion Congress and Exposition, Denver, CO, USA, September 16–20, and approved for publication in the IEEE Transactions on Industry Applications by the Industrial Power Converter Committee of the IEEE Industry Applications Society.

The authors are with the College of Electrical Engineering, Zhejiang University, Hangzhou 310027, China (e-mail: nianheng@zju.edu.cn; zhouyijie@zju.edu.cn).

Color versions of one or more of the figures in this paper are available online at http://ieeexplore.ieee.org.

Digital Object Identifier 10.1109/TIA.2014.2331462

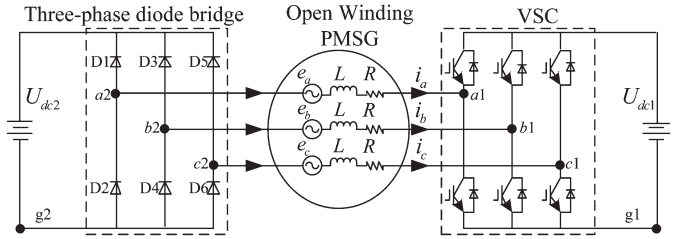

Fig. 2. The open winding PMSG system fed by VSC and diode bridge configuration.

device VA rating. Section III shows the mathematic model of the proposed system. Then, the operation performance with the different dc bus voltage ratios is analyzed in four different cases in Section IV. As a result, the optimized control strategy is selected to obtain the larger linear modulation area. In Section V, the availability of the proposed control strategy for the open winding PMSG system is validated by the experiment results. Finally, conclusions are made in Section VI.

II. Comparisons Between Investigated Topology and Other Converters

The single-side controllable open winding PMSG system topology in this paper is shown in Fig. 2, in which three phase windings of the open winding PMSG are connected to two converters. One converter is a traditional VSC with the controllable switch device, whereas the other is a three-phase diode-bridge-based uncontrollable rectifier. In Fig. 2, two isolated dc voltage sources named as $U_{\rm dc1}$ and $U_{\rm dc2}$ are used as an equivalent to simplify the grid-side configuration.

Compared with the traditional open winding system topology fed with two VSCs, the proposed work only needs half the amount of insulated-gate bipolar transistors (IGBTs) by employing a diode rectifier. The diodes can avoid the driving circuits and snubber circuits so that the system structure is simplified; thus, the proposed work takes a lower expense. On the other hand, the proposed work only needs to deal with one VSC in the control process, which is easier and more reliable than the conventional two-VSC fed system. It can be found that the VSC dc-link voltage $U_{\rm dc1}$ in the proposed work determines the total VA rating of switch devices. Setting the VA rating of the total open winding system as base value, the switch device capacity in the proposed work takes a ratio of $U_{\rm dc1}/(U_{\rm dc1}+U_{\rm dc2})$. However, $U_{\rm dc1}$ in the proposed work should be kept within a reasonable range, which will be introduced in Section IV.

The comparisons of the investigated topology with the traditional open winding topology and the single-VSC fed Y-star topology are shown in Table I. It shows the comparisons from the viewpoint of switch device amounts, converter capacity, and complexity. It can be concluded that the proposed work can enhance the converter reliability and simplify the implementation.

III. Mathematic Model of the Single-Side Controllable Open Winding PMSG System

The mathematic model of the open winding PMSG system in Fig. 2 on the stationary reference frame can be written as [23]

TABLE I
Comparisons of the Proposed Topology With Other Converters

Type of converters	Diode bridge +VSC	VSC+VSC	VSC for Y connected
Total switch device capacity (p.u.)	$U_{\rm dc1}/(U_{\rm dc1}+U_{\rm dc2})$	1	1
Diode amount	6	0	0
Switch device amount	6	12	6
System complexity	simple	complex	simple

$$\begin{cases} u_a = e_a - L\frac{di_a}{dt} - i_aR = S_{a1}U_{\rm dc1} - U_{a2g2} + U_{g1g2} \\ u_b = e_b - L\frac{di_b}{dt} - i_bR = S_{b1}U_{\rm dc1} - U_{b2g2} + U_{g1g2} \\ u_c = e_c - L\frac{di_c}{dt} - i_cR = S_{c1}U_{\rm dc1} - U_{c2g2} + U_{g1g2} \end{cases} \quad (1)$$

where u is the phase voltage; e is the phase electromotive force (EMF); i is the phase current; L is the phase inductance; R is the phase resistance; S is the switching state of each bridge of the VSC; subscripts a, b, and c represent the components in the a, b, and c phases, respectively; subscripts 1 and 2 represent the VSC and the diode bridge; and U_{mn} means the voltage between nodes m and n.

Since the sum of the three phase currents should be zero, the voltage difference between $g1$ and $g2$ can be written as

$$U_{g_1g_2} = \frac{1}{3}\left[(U_{a_2g_2}+U_{b_2g_2}+U_{c_2g_2}) - (S_{a_1}+S_{b_1}+S_{c_1})\,U_{\rm dc_1}\right]. \quad (2)$$

Meanwhile, (1) can be expressed as

$$\mathbf{U} = \mathbf{E} - (Lp+R)\mathbf{I} = \mathbf{U}_1 - \mathbf{U}_2 \quad (3)$$

where $\mathbf{E} = [e_a\ e_b\ e_c]^T$, $\mathbf{I} = [i_a\ i_b\ i_c]^T$, $\mathbf{U} = [u_a\ u_b\ u_c]^T$,

$$\mathbf{U}_1 = \begin{bmatrix} \left(S_{a_1} - \frac{S_{a_1}+S_{b_1}+S_{c_1}}{3}\right)U_{\rm dc_1} \\ \left(S_{b_1} - \frac{S_{a_1}+S_{b_1}+S_{c_1}}{3}\right)U_{\rm dc_1} \\ \left(S_{c_1} - \frac{S_{a_1}+S_{b_1}+S_{c_1}}{3}\right)U_{\rm dc_1} \end{bmatrix}$$

$$\mathbf{U}_2 = \begin{bmatrix} \frac{(2U_{a_2g_2}-U_{b_2g_2}-U_{c_2g_2})}{3} \\ \frac{(2U_{b_2g_2}-U_{a_2g_2}-U_{c_2g_2})}{3} \\ \frac{(2U_{c_2g_2}-U_{a_2g_2}-U_{b_2g_2})}{3} \end{bmatrix}.$$

The ac-side voltage of the three-phase diode bridge is decided by the current direction. For example, if i_a is positive and go through D2, U_{a2g2} is zero. On the contrary, if i_a is negative and go through D1, U_{a2g2} is equal to $U_{\rm dc2}$. Thus,

$$\begin{cases} U_{a2g2} = U_{\rm dc2}{\rm sgn}(i_a) \\ U_{b2g2} = U_{\rm dc2}{\rm sgn}(i_b) \\ U_{c2g2} = U_{\rm dc2}{\rm sgn}(i_c) \end{cases} \quad (4)$$

where

$${\rm sgn}(i_j) = \begin{cases} 1, & \text{if } (i_j > 0), \\ 0, & \text{if } (i_j < 0), \end{cases} \qquad j = a, b, c.$$

TABLE II
RELATIONSHIP BETWEEN THE CURRENT DIRECTION AND $V_{\rm II}$

current direction			output vector
i_a	i_b	i_c	$V_{\rm II}$
P	N	N	(011)
P	P	N	(001)
P	N	P	(010)
N	P	N	(101)
N	N	P	(110)
N	P	P	(100)

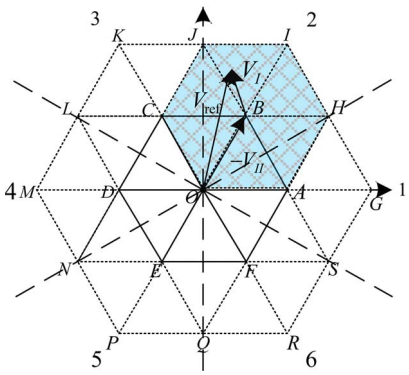

Fig. 3. Vector scheme of the proposed configuration when $U_{\rm dc1} = U_{\rm dc2}$.

Thus, when the d-axis is aligned with the rotor flux linkage direction, the mathematic model of the open winding PMSG on the dq synchronous rotating frame can be written as

$$\begin{cases} u_d = u_{d1} - u_{d2} = -i_d R - L_d \frac{di_d}{dt} + \omega_r L_q i_q \\ u_q = u_{q1} - u_{q2} = -i_q R - L_q \frac{di_q}{dt} - \omega_r L_d i_d + \omega_r \psi_r \\ P_e = \frac{3}{2}\omega_r \left[\psi_r i_q + (L_d - L_q) i_d i_q\right] \end{cases} \quad (5)$$

where ω_r is the generator electrical angular speed; Ψ_r is the rotor magnetic flux produced by the permanent magnet; subscripts d and q represent the d- and q-axis components, respectively; and P_e is the power output by the PMSG system.

Furthermore, according to (5), when pulsewidth modulation (PWM) is applied in the control scheme of the open winding PMSG system, the reference voltage vector $V_{\rm ref}$ for the open winding PMSG system can be expressed as

$$\begin{cases} V_{\rm ref} = V_I - V_{\rm II} \\ V_{\rm ref} = u_d + j u_q \\ V_I = u_{d1} + j u_{q1}, V_{\rm II} = u_{d2} + j u_{q2} \end{cases} \quad (6)$$

where V_I and $V_{\rm II}$ is the voltage vector modulated by the VSC and the diode bridge, respectively.

It should be noted that the voltage vector $V_{\rm II}$ is decided by the ac-side current direction in the three-phase diode bridge. As the three phase currents will not be in the same direction at one time, the diode bridge can provide six different voltage vector statues for the open winding PMSG. The relationship between the current direction and $V_{\rm II}$ is shown in Table II, in which N and P represent the phase current in the negative and positive directions, respectively. The output vector means the corresponding voltage vector generated by the diode bridge.

According to the six different output voltage vectors and the current direction of the diode bridge, Fig. 3 shows the vector scheme of the open winding PMSG system with the integration of full-controlled and uncontrolled converter in the case that $U_{\rm dc1} = U_{\rm dc2}$, in which the current vector is departed into six regions by the dashed line, which are named regions 1–6. Considering that $U_{\rm dc1} = U_{\rm dc2}$, if i_a and i_b are positive, while i_c is negative, $V_{\rm II}$ can be expressed as (001), and the current vector locates in section 2. Meanwhile, the controllable VSC could modulate voltage vector around the center point B. Then, $V_{\rm ref}$ can be modulated in the range of the blue hexagon.

Because only one controllable converter is employed in the open winding PMSG system, the common-mode voltage will inevitably occur. However, since the investigated open winding system is supplied with two isolated dc buses and a zero-sequence circuit is nonexistent, the sum of the three phase stator currents is zero at any instant according to Kirchhoff's law. Thus, the proposed work makes no contribution to the common-mode current. The investigation of this paper is focused on the control strategy and analysis of the open winding PMSG system with single-side controllable converter; the further analysis on common-mode voltage and current will be accomplished in the future.

IV. STUDY ON DIFFERENT DC-LINK RATIOS

The dc-link ratio of two converters is an important parameter for open winding system, which affects the system output voltage characteristic and power distribution on the two converters. In the previous research, it can be found that the conventional open winding PMSG system with two isolated dc voltages could achieve various multilevel effects with different dc-link ratio values, i.e., $U_{\rm dc2} : U_{\rm dc1}$. In [24], a four-level voltage waveform was achieved by employing the dc voltage ratio 2 : 1, and the lower current harmonic content can be obtained. A larger range of dc-link ratio from 0 : 1 to 2 : 1 was clarified in [25], in which series modulation results with different ratio values were analyzed. Thus, it is different from the conventional multilevel implementation method that the open winding PMSG could achieve multilevel modulation effect by changing dc-link ratio without employing the corresponding multilevel converters.

Nevertheless, according to the aforementioned analysis, the open winding PMSG system with the integration of full-controlled and uncontrolled converter could only work in a limited modulation region due to the clamped voltage vector by the diode bridge. The limited region determines the available voltage vector modulation range. Thus, by investigating the operation mechanism on the different dc voltage ratios, the optimized control strategy of the single-side controllable open winding system can be achieved. In addition, because the total switch devices power rating is decided by $U_{\rm dc2}$, it is helpful to obtain the cost-effective system for the single-side controllable open winding PMSG system by studying the influence of lower $U_{\rm dc2}$ on the system operation performance. Therefore, it is meaningful to investigate the dc-link ratio impact on the single-side controllable open winding PMSG system.

Fig. 4 shows the voltage vector diagram modulated by the single-side controllable open winding PMSG system with different dc bus voltage ratios when the current vector locates in region 2. In Fig. 4, hexagons formed by the voltage vectors of the diode bridge are named as auxiliary hexagons, whereas the

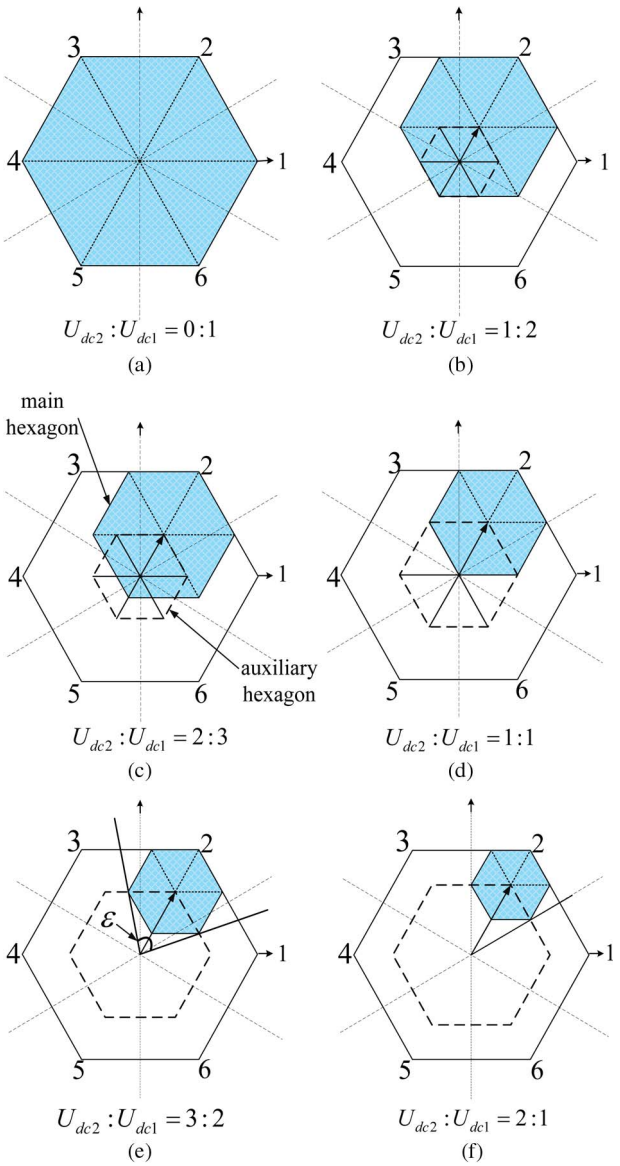

Fig. 4. Vector diagram of the proposed configuration with different voltage ratios.

hexagons formed by the VSC are named as main hexagons. The auxiliary hexagons are presented by the fold line, whereas the main hexagons are filled with blue background. Thus, the main hexagons indicate the available modulation area to obtain the voltage vector reference. If $U_{\rm dc2}:U_{\rm dc1}=0:1$, no auxiliary hexagons can be modulated, the system will work as the traditional two-level converter system shown in Fig. 4(a), in which the diode plays the role as a neutral point of the Y-connect. The modulation region is the whole main hexagon, same as a two-level VSC. As $U_{\rm dc2}$ increases, the main hexagon area decreases. In the case that $U_{\rm dc2}:U_{\rm dc1}=1:2$, the main hexagon can only overlap the whole auxiliary hexagon, as shown in Fig. 4(b), which means that the voltage vectors combined by VSC can cover the voltage vector region by diode bridge, whereas in the case that $U_{\rm dc2}:U_{\rm dc1}=2:3$, the main hexagon can only overlap part of the auxiliary hexagon, as shown in Fig. 4(c). When $U_{\rm dc2}:U_{\rm dc1}=1:1$, the voltage vector scheme is similar to a three-level one, as shown in Fig. 4(d), in which O point is on the boundary of the main hexagon, which means zero vectors can still be modulated. While $U_{\rm dc2}:U_{\rm dc1}>1:1$, the available voltage vector cannot cover region 2 because no zero vectors could be implemented. When $U_{\rm dc2}:U_{\rm dc1}=3:2$, the voltage vector reference is limited in the phase angle region, as shown in Fig. 4(e). Beyond the phase region, the voltage vector could not be modulated. When $U_{\rm dc2}:U_{\rm dc1}=2:1$, the angle of the modulated range is equal to that of the range in section 2, which means 60°, as shown in Fig. 4(f). In this case, the voltage vector modulation region is just successive for the continuous six current regions; thus, the open winding PMSG is still controllable. When $U_{\rm dc2}:U_{\rm dc1}>2:1$, the voltage vector modulation region is not successive for the continuous six current regions, which means that the open winding PMSG is not controllable and the system could not keep stable work state normally. Thus, it can be seen that different dc-link ratios decide the size of the main hexagon area, as shown in Fig. 4(a)–(f). The limited modulation region indicates that the voltage vector amplitude is influenced by the angle between voltage vector and current vector. Therefore, the power factor angle is a key factor to determine the maximum linear modulation index for the open winding PMSG system when working on the single-side controllable converter.

A. Modulation Region Analysis

The phasor diagram of the open winding PMSG is shown in Fig. 5. It can be seen that the power factor angle between the current and voltage vectors has three different relationship: current leading voltage [see Fig. 5(a)], current in phase with voltage [see Fig. 5(b)], and current lagging voltage [see Fig. 5(c)]. The absolute value of the power factor angle should be less than 90° in order to ensure the open winding PMSG system working in the generator condition.

In Fig. 5, the voltage equation of the open winding PMSG system can be expressed as

$$V_{\rm ref}=E-jX_dI_q-jX_qI_d. \tag{7}$$

It should be noted that the available voltage vector will change as dc-link voltage ratio changes. In order to make a detailed analysis, it is discussed in four cases with different ratio ranges: 1) $U_{\rm dc2}:U_{\rm dc1}<1:2$; 2) $1:2<U_{\rm dc2}:U_{\rm dc1}<1:1$; 3) $U_{\rm dc2}:U_{\rm dc1}=1:1$; and 4) $1:1<U_{\rm dc2}:U_{\rm dc1}<2:1$. These four cases cover the ratio from $0:1$ to $2:1$. As aforementioned, the voltage vector modulation region for six current regions is discontinuous with the ratio exceeding $2:1$, which means a failed work condition for the open winding PMSG.

1) $U_{\rm dc2}:U_{\rm dc1}<1:2$: When the current vector is located in region 2, the voltage vector modulation region that can be achieved is the main hexagon region shown in Fig. 6.

If the current vector is in phase with the voltage vector, the linear modulation range allows the maximum voltage reference $(V_{\rm ref})_{\max}$ shown as OT. If the current is lagging (or leading) the voltage, based on the symmetry, it can be inferred that, as the current vector reaches the boundary OT, the corresponding voltage vector should locate in the shadow region between OT and OW. Thus, in order to implement the open winding PMSG

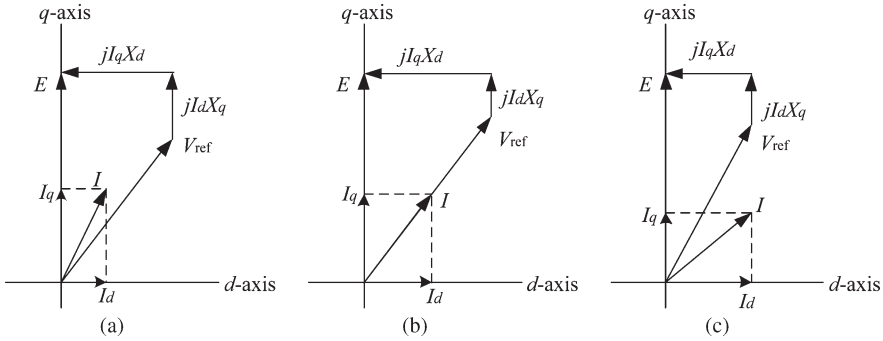

Fig. 5. Phasor diagram of operating principle of the proposed system. (a) Current leading voltage. (b) Current in phase with voltage. (c) Current lagging voltage.

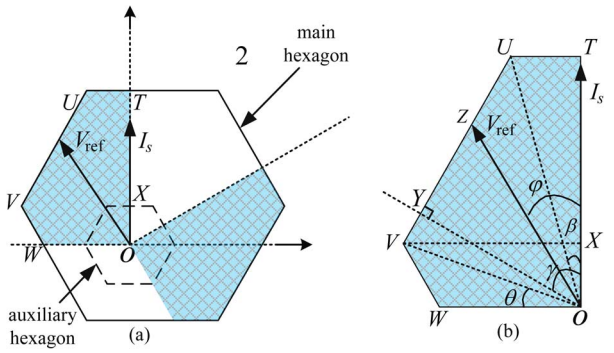

Fig. 6. Modulation region analysis on $U_{\mathrm{dc2}} : U_{\mathrm{dc1}} < 1 : 2$. (a) Phasor diagram. (b) Amplification of shadow area.

working in the linear modulation region, V_{ref} should be inside of the shadow region, and the power factor angle φ decides the maximum voltage reference, i.e., $(V_{\mathrm{ref}})_{\max}$. Fig. 6(b) shows the available voltage vector range when current vector is located on OT. In Fig. 6(b), it is shown that the boundary trajectory swerves in three different angle thresholds, namely, β, γ, and θ, which can be calculated as

$$\begin{cases} \beta = \arctan\left(\dfrac{|UT|}{|OT|}\right) = \arctan\left[\dfrac{\frac{1}{3}U_{\mathrm{dc1}} - \frac{1}{3}U_{\mathrm{dc2}}}{\frac{\sqrt{3}}{3}(U_{\mathrm{dc1}} + U_{\mathrm{dc2}})}\right] \\ \theta = \arctan\left(\dfrac{|OX|}{|VX|}\right) = \arctan\left[\dfrac{\frac{\sqrt{3}}{3}U_{\mathrm{dc2}}}{\frac{2}{3}U_{\mathrm{dc1}} - \frac{1}{3}U_{\mathrm{dc2}}}\right], \quad \gamma = 60^\circ. \end{cases} \tag{8}$$

In order to obtain the relationship between φ and $(V_{\mathrm{ref}})_{\max}$, the length between zero vector point O and the boundary could be solved as $(V_{\mathrm{ref}})_{\max}$. As power factor angle changes, the $(V_{\mathrm{ref}})_{\max}$ varies along with the modulation region boundary. It can be deduced as

$$(V_{\mathrm{ref}})_{\max} = \begin{cases} \dfrac{\sqrt{3}(U_{\mathrm{dc1}}+U_{\mathrm{dc2}})}{3}, (|\varphi| < \beta) \\ \min\left[\dfrac{\sqrt{3}}{3}(U_{\mathrm{dc1}} + U_{\mathrm{dc2}}), \dfrac{\frac{\sqrt{3}}{3}U_{\mathrm{dc1}}}{\cos(60^\circ - |\varphi|)}\right], (\beta < |\varphi| < \gamma) \\ \dfrac{\sqrt{3}}{3}U_{\mathrm{dc1}}, (\gamma < |\varphi| < 90^\circ - \theta) \\ \min\left[\dfrac{\sqrt{3}U_{\mathrm{dc1}}}{3}, \dfrac{\sqrt{3}U_{\mathrm{dc1}} - \sqrt{3}U_{\mathrm{dc2}}}{3\sin(|\varphi| - 30^\circ)}\right], (90^\circ - \theta < |\varphi| < 90^\circ). \end{cases} \tag{9}$$

2) $1 : 2 < U_{\mathrm{dc2}} : U_{\mathrm{dc1}} < 1 : 1$*:* If the dc-link ratio is $1 : 2 < U_{\mathrm{dc1}} : U_{\mathrm{dc2}} < 1 : 1$, the modulation region achieved is shown in Fig. 7. In this case, two different angle thresholds β and θ have the same definition as that in case 1.

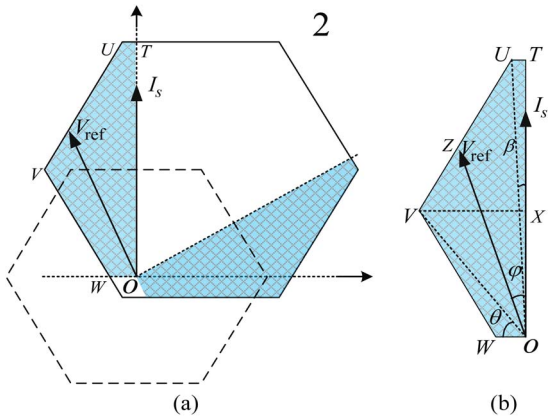

Fig. 7. Modulation region analysis on $1 : 2 < U_{\mathrm{dc2}} : U_{\mathrm{dc1}} < 1 : 1$. (a) Phasor diagram. (b) Amplification of shadow area.

It can be inferred from Fig. 7 that the relationship of power factor angle φ and $(V_{\mathrm{ref}})_{\max}$ can be given as

$$(V_{\mathrm{ref}})_{\max} = \begin{cases} \dfrac{\sqrt{3}(U_{\mathrm{dc1}}+U_{\mathrm{dc2}})}{3}, (|\varphi| < \beta) \\ \min\left[\dfrac{\sqrt{3}}{3}(U_{\mathrm{dc2}}+U_{\mathrm{dc1}}), \dfrac{\frac{\sqrt{3}}{3}U_{\mathrm{dc1}}}{\cos(60^\circ - |\varphi|)}\right], (\beta < |\varphi| < 90^\circ - \theta) \\ \dfrac{\sqrt{3}U_{\mathrm{dc1}} - \sqrt{3}U_{\mathrm{dc2}}}{3\sin(|\varphi| - 30^\circ)}, (90^\circ - \theta < |\varphi| < 90^\circ). \end{cases} \tag{10}$$

3) $U_{\mathrm{dc2}} : U_{\mathrm{dc1}} = 1 : 1$*:* If the dc-link ratio $U_{\mathrm{dc2}} : U_{\mathrm{dc1}} = 1 : 1$, the zero vector could still be modulated. In addition, the power factor angle is limited within the range of 30°, as shown in Fig. 8.

In addition, it can be inferred from Fig. 8 that, in the linear modulation range, the relationship of power factor angle φ and $(V_{\mathrm{ref}})_{\max}$ can be given as

$$(V_{\mathrm{ref}})_{\max} = |OZ| = \frac{\sqrt{3}}{6\sin(150^\circ - |\varphi|)}(U_{\mathrm{dc1}} + U_{\mathrm{dc2}}), \quad (|\varphi| \le 30^\circ). \tag{11}$$

4) $1 : 1 < U_{\mathrm{dc2}} : U_{\mathrm{dc1}} < 2 : 1$*:* If the dc-link ratio $1 : 1 < U_{\mathrm{dc2}} : U_{\mathrm{dc1}} < 2 : 1$, the available voltage vector cannot cover region 2 because no zero vectors could be implemented.

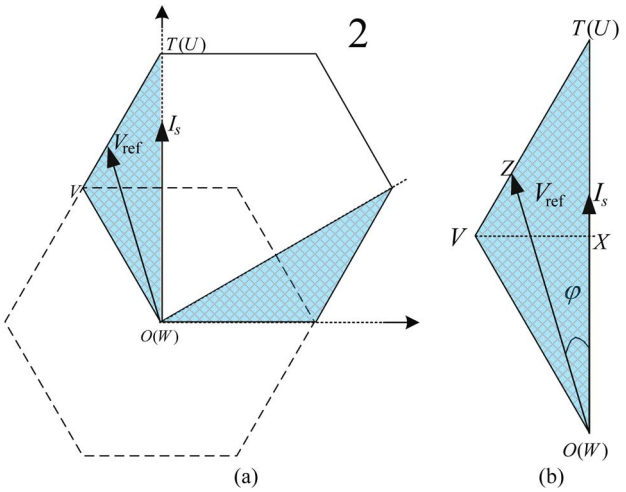

Fig. 8. Modulation region analysis on $U_{dc2} : U_{dc1} = 1 : 1$. (a) Phasor diagram. (b) Amplification of shadow area.

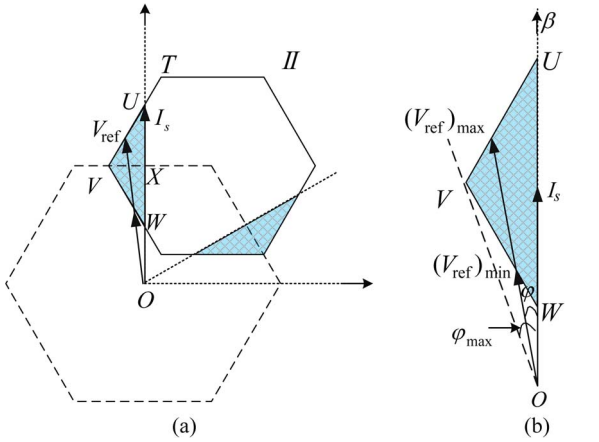

Fig. 9. Modulation region analysis on $1 : 1 < U_{dc2} : U_{dc1} < 2 : 1$. (a) Phasor diagram. (b) Amplification of shadow area.

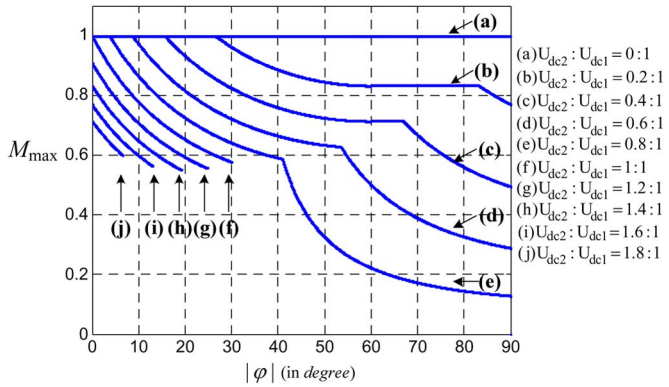

Fig. 10. Relationship between power factor angle and M_{max} with different dc-link ratios.

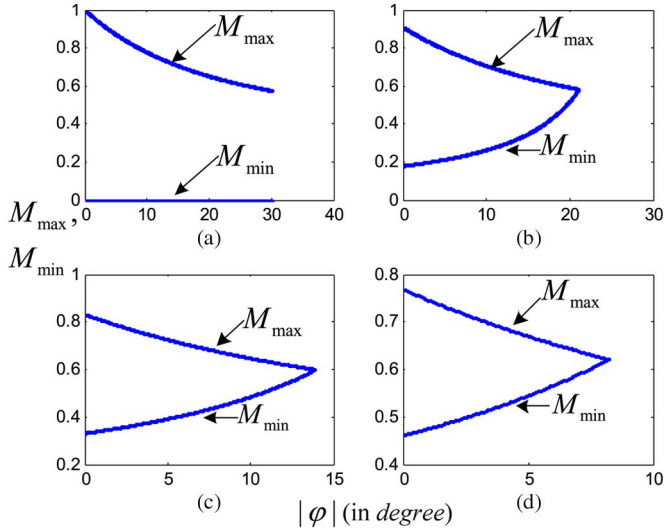

Fig. 11. Relationship between power factor angle and M_{max}, M_{min}. (a) $U_{dc2} : U_{dc1} = 1 : 1$. (b) $U_{dc2} : U_{dc1} = 1.2 : 1$. (c) $U_{dc2} : U_{dc1} = 1.4 : 1$. (d) $U_{dc2} : U_{dc1} = 1.6 : 1$.

Therefore, the linear modulation range is limited by the maximum voltage reference $(V_{ref})_{max}$ and the minimum voltage reference $(V_{ref})_{min}$. When the current vector is leading or lagging the voltage vector, based on the symmetry, it can be inferred from Fig. 9 that, in the linear modulation range, the power factor angle φ and $(V_{ref})_{max}$ and $(V_{ref})_{min}$ have a limitation as

$$\begin{cases} |\varphi_{max}| \le \arctan\left(\frac{2U_{dc1}-U_{dc2}}{\sqrt{3}U_{dc2}}\right) \\ (V_{ref})_{max} = \frac{\frac{\sqrt{3}}{3}U_{dc1}}{\sin(30°+|\varphi|)} \\ (V_{ref})_{min} = \frac{\frac{\sqrt{3}}{3}(U_{dc2}-U_{dc1})}{\sin(30°-|\varphi|)} \end{cases} . \quad (12)$$

Assuming voltage base value $V_{base} = \sqrt{3}(U_{dc1} + U_{dc2})/3$ and the modulation index $M = V_{ref}/V_{base}$, Fig. 10 shows the relationship between power factor angle φ and the maximum modulation index M_{max} on the different dc-link ratios. It can be seen that, when $U_{dc2} : U_{dc1} < 1 : 1$, the modulation region can cover the power factor angle changing from $0°$ to $90°$. While $U_{dc2} : U_{dc1} > 1 : 1$, the power factor angle is limited in a certain range to achieve the available modulation region, as shown with the line (f–j). In Fig. 10, it is shown that, in all cases from $U_{dc2} : U_{dc1} = 0 : 1$ to $U_{dc2} : U_{dc1} = 2 : 1$, the unity power factor can give out the maximum modulation index, which means that the maximum voltage utilization can be achieved.

Fig. 11 shows the relationship between the power factor angle φ and M_{max}, M_{min} on the different dc voltage ratios in the case $U_{dc2} : U_{dc1} \ge 1 : 1$. Fig. 11(a) gives the relationship in the case $U_{dc2} : U_{dc1} = 1 : 1$. It can be seen that the available power factor angle region is from $0°$ to $30°$. In Fig. 11(b)–(d), the cross point of the curve M_{max} and M_{min} represents the maximum power factor angle φ that could be achieved. Thus, the available power factor angle operation region decreases as the dc-link ratio increases. Therefore, it can be seen that the available modulation region will diminish as the dc voltage ratio becomes larger.

From the analysis above, it can be concluded that unity power factor control method is the optimized control strategy for the single-side controllable open winding PMSG system to achieve the maximum voltage vector modulation range. As power factor angle increases, the available M_{max} will decrease correspondingly, as shown in Figs. 10 and 11.

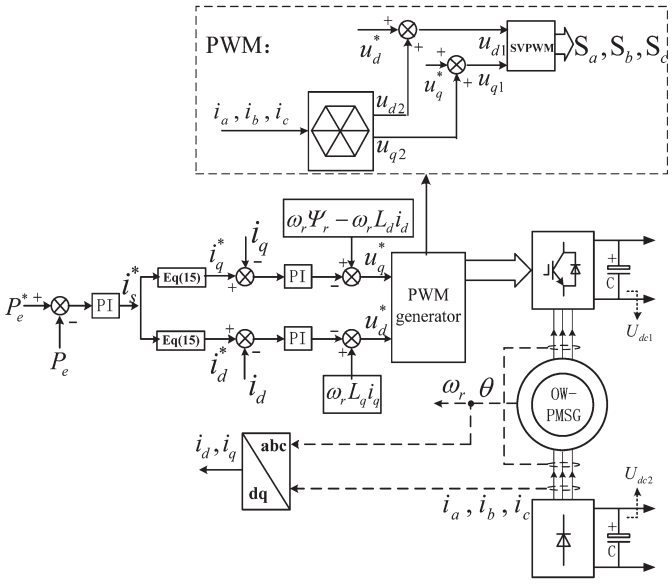

Fig. 12. Control scheme of the open winding PMSG system.

B. System Control Strategy

The control scheme of the single-side controllable open winding PMSG system is shown as Fig. 12. With the unity power factor control method, the current reference i_S^* can be achieved by the power loop control regulator in (13). The d- and q-axis current references are obtained by (14). Based on the current loop control regulator, the d- and q-axis voltage references could be calculated in (15) and (16). When $V_{\rm ref}$ is calculated, the voltage vector output by the diode bridge could be obtained by the three phase stator current direction. Then, the reference voltage for VSC modulation can be calculated from (6). Thus,

$$i_s^* = K_{p1}\left(P_e^* - P_e\right) + K_{i1}\int\left(P_e^* - P_e\right)dt \tag{13}$$

$$i_d^* = \frac{-\psi_r + \sqrt{\psi_r^2 - 4(L_d - L_q)L_q I_s^{*2}}}{2(L_d - L_q)}$$

$$i_q^* = \sqrt{I_s^{*2} - i_d^{*2}} \tag{14}$$

$$u_q^* = \omega_r\psi_r - \omega_r L_d i_d - K_{p2}\left(i_q^* - i_q\right) - K_{i2}\int\left(i_q^* - i_q\right)dt$$

(15)

$$u_d^* = \omega_r L_q i_q - K_{p2}\left(i_d^* - i_d\right) - K_{i2}\int\left(i_d^* - i_d\right)dt \tag{16}$$

where K_{p1} and K_{i1} represent the proportional and integral gains of the power control regulator, respectively; whereas K_{p2} and K_{i2} represent the proportional and integral gains of the current control regulator, respectively.

As written in Section IV, if the voltage reference locates outside the linear modulation region, the open winding system operation will be unstable. Thus, the modulation index should be automatically limited within the available modulation range in case of the different dc-link ratios. Thus, it can be inferred that

$$M_{\min} \le M \le M_{\max}. \tag{17}$$

In the practical operation, in order to achieve the stable operation of open winding PMSG system, a modulation index limiter can be applied to guarantee that the final modulation index is limited in the range restricted by $M_{\min}$ and $M_{\max}$.

TABLE III
OPEN WINDING PMSG PARAMETERS

Parameter	value	Parameter	value
Rated power $P_{\rm n}$	1kW	Rated speed n	80r/min
Rated phase voltage	133V	Rated phase current	2.5A
Rated frequency $f_{\rm n}$	10.67Hz	d-axis inductance $L_{\rm d}$	77.56mH
Stator $R_{\rm s}$	1.1Ω	q-axis inductance $L_{\rm q}$	107.4mH
Pole number $n_{\rm p}$	8		

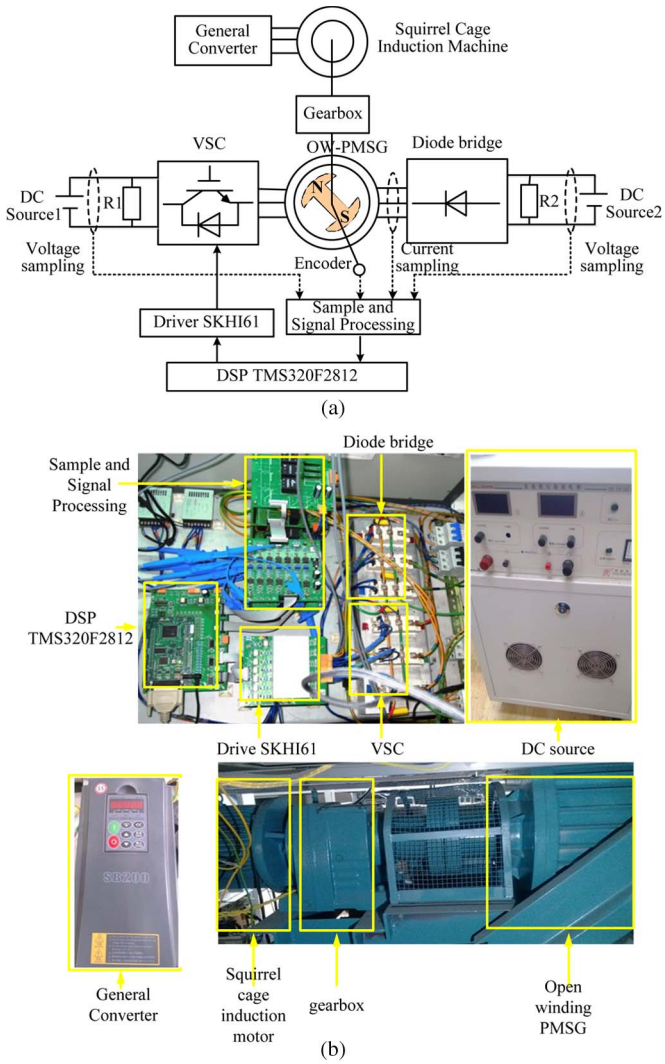

Fig. 13. Experimental setup. (a) Block diagram. (b) Hardware setup.

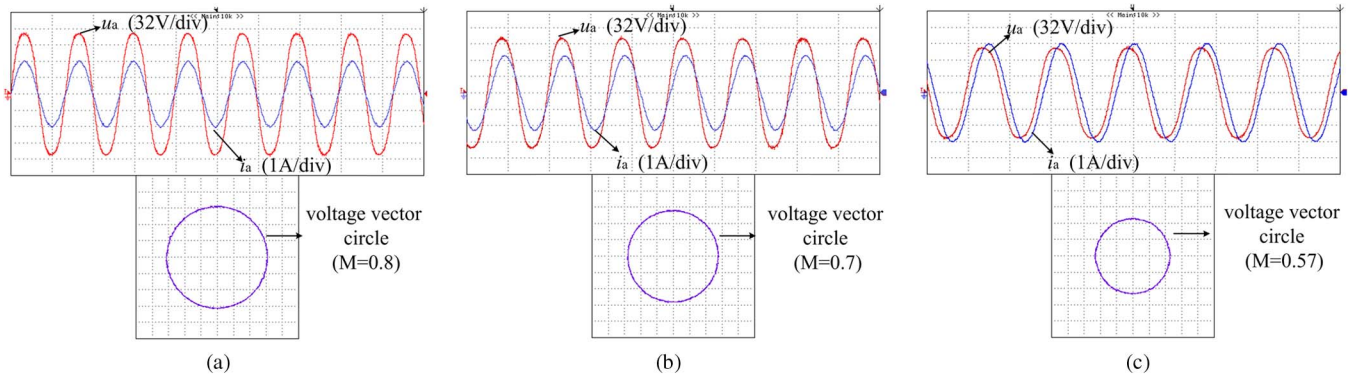

Fig. 14. Experimental results of three conditions under the case that $U_{\rm dc2} : U_{\rm dc1} = 1 : 1 (U_{\rm dc1} = 150$ V, $U_{\rm dc2} = 150$ V). (a) Voltage in phase with current with $M = 0.8$. (b) Voltage leading current 15° with $M = 0.7$. (c) Voltage leading current 30° with $M = 0.57$.

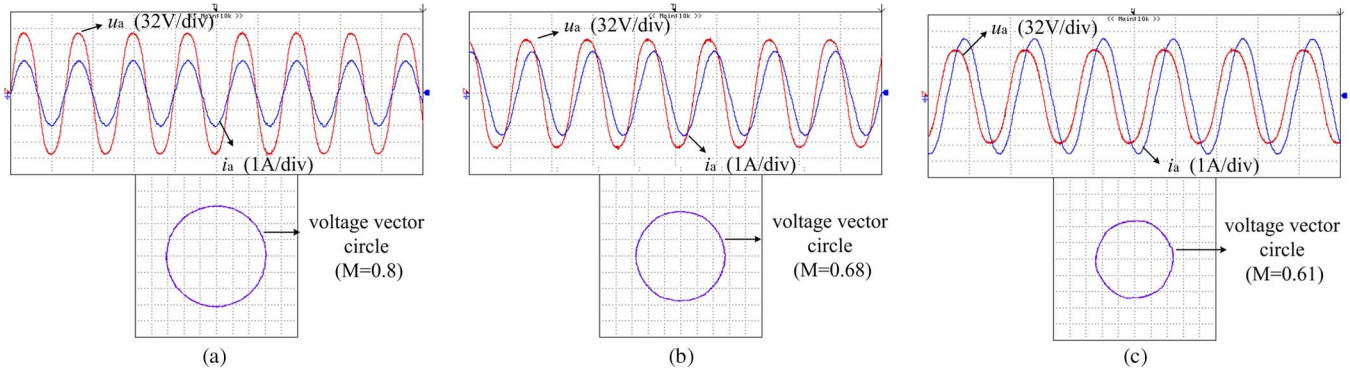

Fig. 15. Experimental results of three conditions under the case that $U_{\rm dc2} : U_{\rm dc1} = 2 : 3 (U_{\rm dc1} = 180$ V, $U_{\rm dc2} = 120$ V). (a) Voltage in phase with current with $M = 0.8$. (b) Voltage leading current 30° with $M = 0.68$. (c) Voltage leading current 45° with $M = 0.61$.

V. Experimental Results

The experimental system of 1-kW open winding PMSG system with the integration of full-controlled and uncontrolled converter is developed in a laboratory. In the experimental system, the open winding PMSG is driven by a 1.5-kW squirrel-cage induction machine, and a gearbox with the ratio 17.08 is used as a mechanical interface. The induction machine is driven by a general converter. The open winding PMSG parameters are shown in Table III. Two isolated adjustable dc power supplies are used to establish the dc bus voltage. The VSCs are built with SEMIKRON SKM75GB124DE IGBTs. The VSC controller is implemented based on TMS320F2812, and the driver for IGBT is SEMIKRON SKHI61. The sampling frequency is kept at 10 kHz, and the switching frequency of the IGBTs is 5 kHz. The experimental waveforms acquisition is obtained by a YOKOGAWA DL750 scope recorder. Two 20-Ω resistances are paralleled with dc sources to work as the load to consume the energy generated by the open winding PMSG. The block diagram of experiment system is shown in Fig. 13(a), and the experimental hardware setup is shown in Fig. 13(b).

In the practical applications, the grid-side converter will be employed as the interface between the grid and the dc bus to implement the power flow from the open winding PMSG to the grid. Thus, the different ratios of dc-link voltages can be implemented by the grid-side converter control. The keynote of this paper is to investigate the operation impact with the different dc-link, and the two adjustable dc sources are applied to simplify the open winding PMSG system.

In the PMSG system, the back EMF is proportional to the rotor speed. Thus, the magnitude of voltage vector varies as the rotor speed varies. Thus, in order to validate the available modulation region and the proposed optimized control strategy of unity power factor control, the rotor speed is changed to match the modulation index. On the other hand, the d- and q-axis current references are set according to the constant power factor angle control to validate the relationship between power factor and modulation index.

Fig. 14 shows the experimental results of a phase voltage and current in the case $U_{\rm dc2} : U_{\rm dc1} = 1 : 1$ and the voltage vector circles of the open winding PMSG system. $U_{\rm dc1}$ and $U_{\rm dc2}$ are both set as 150 V. On the operation condition of the same active power output reference with 360 W, the experimental results based on the unity power factor control and constant 15° and 30° power factor angle control are shown in Fig. 14(a)–(c). Because the unity power factor control can allow $M_{\rm max} = 1$, a stable work state with $M = 0.8$ is obtained in Fig. 14(a). Theoretically, $M_{\rm max}$ on the constant 15° and 30° power factor angle control are 0.707 and 0.577 from (11). The experimental results in Fig. 14(b) and (c) give the operation state as the critical point with modulation index as 0.7 and 0.57, which is almost equal to the maximum modulation index. If the modulation index is larger than 0.707 and 0.577, the open winding system could not work normally in the experiment. The stable work condition

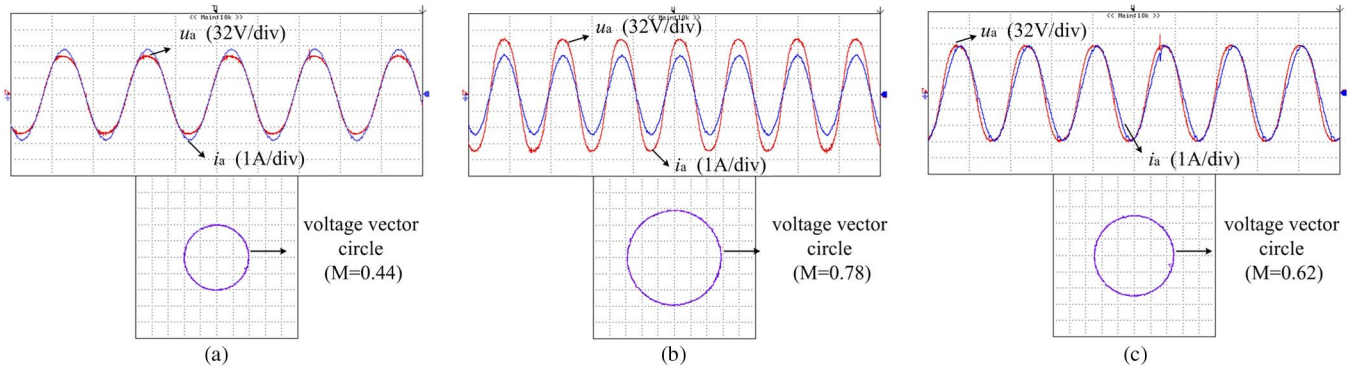

Fig. 16. Experimental results of three conditions under the case that $U_{dc2} : U_{dc1} = 3 : 2 (U_{dc1} = 120$ V, $U_{dc2} = 180$ V). (a) Voltage in phase with current with $M_{min} = 0.44$. (b) Voltage in phase with current with $M_{max} = 0.78$. (c) Voltage leading current 10° with $M = 0.62$.

validates the range of power factor angle and the correctness of the relationship between power factor angle and M_{max}. It should be noted that the voltage drop on stator resistance exists in the experiment,. The experimental result analysis with unity power factor control shows that the power factor is up to 0.997. Therefore, the resistive voltage drop does not affect the unity power factor implementation.

Fig. 15 shows the experimental results of a phase voltage and current and the voltage vector circles in the case $U_{dc2} : U_{dc1} = 2 : 3$, in which U_{dc1} and U_{dc2} are set to 120 and 180 V, respectively. On the condition of the same power output with 360 W, the experimental results on the unity power factor control and constant 30° and 45° power factor angle control are shown in Fig. 15(a)–(c). The unity power factor control allows $M_{max} = 1$, and a stable work state with $M = 0.8$ is shown in Fig. 15(a). Theoretically, the M_{max} for constant 30° and 45° power factor angle control are 0.693 and 0.621 from (10). The experimental results in Fig. 15(b) and (c) give the operation condition as the critical point with $M_{max} = 0.68$ and 0.61. If the modulation index is larger than these two values, the open winding PMSG system could not work normally.

Fig. 16 gives the experimental results of a phase voltage and current waveforms and voltage vector circles in the case $U_{dc2} : U_{dc1} = 3 : 2$. U_{dc1} and U_{dc2} are set to 180 and 120 V, respectively. In the condition of the same power output with 360 W, it gives the comparison on the unity power factor control with both M_{max} and M_{min} and constant 10° power factor angle control, which is the maximum angle that can be achieved. In theory, the M_{max} and M_{min} for unity power factor control are 0.8 and 0.4 from (12). In addition, the maximum power factor angle is 10.6° with $M = 0.62$. The experimental results in Fig. 16(a) and (b) give the operation condition as critical point, showing M_{max} and M_{min} as 0.78 and 0.4 with unity power factor control. In addition, constant 10° power factor angle control shown in Fig. 16(c) gives the modulation index as 0.62, which matches the theory result accurately.

The comparison of theoretical and experimental M_{max} and M_{min} in the linear modulation region is shown in Fig. 17(a) and (b). It can be seen that the experimental results can match theoretical analysis well for all the three cases: 1) $U_{dc2} : U_{dc1} = 2 : 3$; 2) $U_{dc1} : U_{dc2} = 1 : 1$; and 3) $U_{dc1} : U_{dc2} = 3 : 2$. M_{max} and M_{min} can be achieved with $\varphi = 0$. When the power factor angle increases, the available modulation region decreases. Thus, unity power factor control method is the optimized control method for the open winding PMSG system with the integration of the VSC and the diode bridge. Meanwhile, in the case $U_{dc1} : U_{dc2} = 1 : 1$, the total power rating for switch device could be reduced to the minimum, and the available modulation region from 0 to 1 can be achieved.

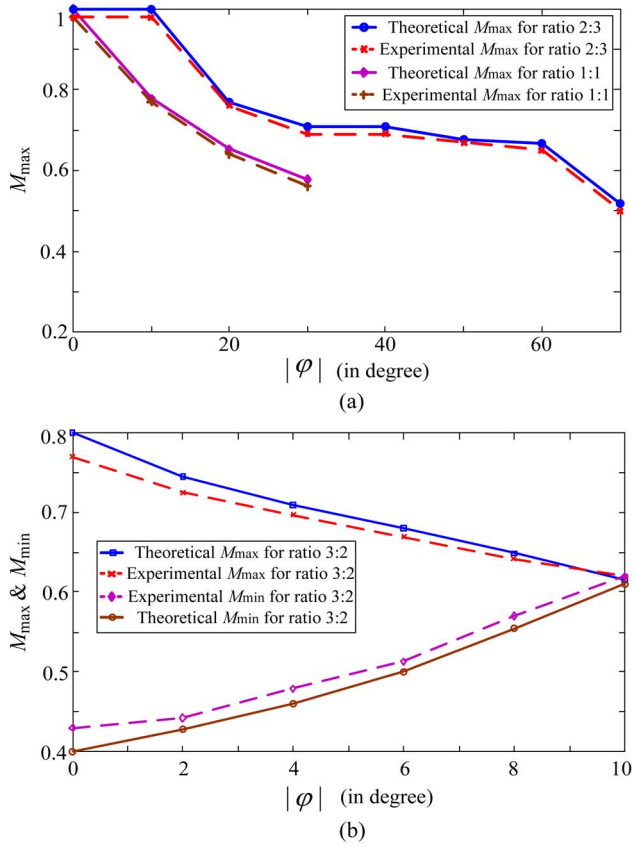

Fig. 17. Comparison of theoretical and experimental M_{max} and M_{min} values in different dc-link ratios.

Based on the unity power factor control, the dynamic response with 50% active power step changes from 1000 to 500 W is shown in Fig. 18, with $U_{dc2} : U_{dc1} = 1 : 1$. It can be seen that P_e can follow the power reference value with $\pm 2.73\%$ control error. The dynamic response time can be controlled in 200 ms.

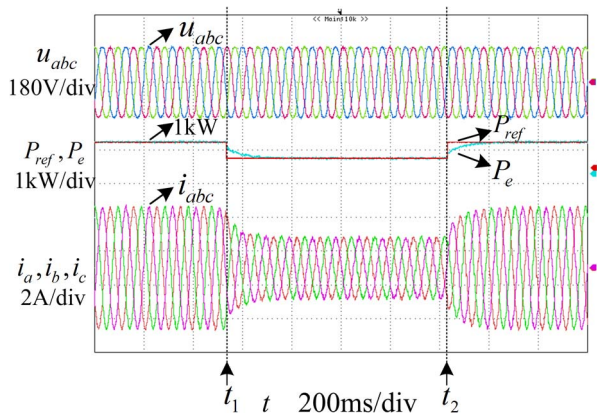

Fig. 18. Dynamic response of the open winding PMSG with 50 power step change.

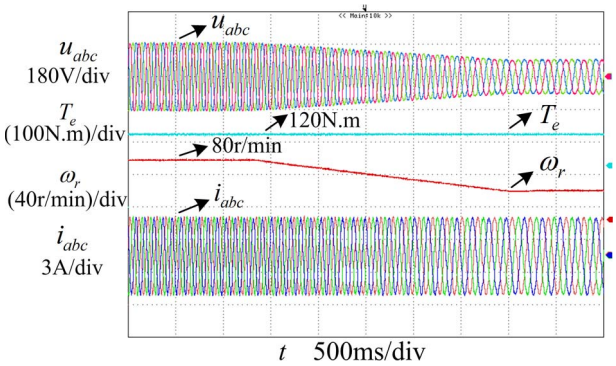

Fig. 19. Dynamic response of the open winding PMSG with 50% speed changes.

Fig. 19 shows the dynamic response with 50% speed step changes from 80 to 40 r/min with constant torque reference in the case that $U_{\rm dc1} : U_{\rm dc2} = 1 : 1$. As the rotor speed changes, the voltage amplitude reduces due to the back EMF decreasing. In addition, the torque ripple is limited in $\pm 2.54\%$. It can be seen that the open winding PMSG can keep stable operation by the unity power factor control strategy.

VI. Conclusion

This paper has investigated the open winding PMSG system with the integration of full-controlled and uncontrolled converter. Due to the clamped voltage vector by the current direction in the diode bridge, the open winding PMSG can only work in a limited modulation region. Based on the analysis on the available modulation index on the different dc voltage ratios, the unity power factor control strategy is the optimized control for the open winding PMSG system with single-side controllable VSC, which can achieve the maximum voltage modulation range. The experimental results validate the correctness of the theoretical analysis on the open winding PMSG system.

References

[1] J. A. Baroudi, V. Dinavahi, and A. M. Knight, "A review of power converter topologies for wind generators," *Renew. Energy*, vol. 32, no. 14, pp. 2369–2385, Nov. 2007.

[2] Z. Chen, J. M. Guerrero, and F. Blaabjerg, "A review of the state of the art of power electronics for wind turbines," *IEEE Trans. Power. Electron.*, vol. 24, no. 8, pp. 1859–1875, Aug. 2009.

[3] F. Blaabjerg, M. Liserre, and K. Ma, "Power electronics converters for wind turbine systems," *IEEE Trans. Ind. Appl.*, vol. 48, no. 2, pp. 708–719, Feb./Apr. 2012.

[4] D. S. Oliveira, M. M. Reis, and C. Silva, "A three-phase high frequency semicontrolled rectifier for PM WECS," *IEEE Trans. Power. Electron.*, vol. 25, no. 3, pp. 677–685, Mar. 2010.

[5] V. T. Somasekhar, K. Gopakumar, and M. R. Baiju, "A multilevel inverter system for an induction motor with open-end windings," *IEEE Trans. Ind. Electron.*, vol. 52, no. 3, pp. 824–836, Jun. 2005.

[6] Y. Wang, D. Panda, T. A. Lipo, and D. Pan, "Open winding power conversion systems fed by half-controlled converters," *IEEE Trans. Power. Electron.*, vol. 28, no. 5, pp. 2427–2436, May 2013.

[7] V. Barry and S. Veeramraju, "A dual inverter fed four-level open-end winding induction motor drive with a nested rectifier inverter," *IEEE Trans. Ind. Informat.*, vol. 9, no. 2, pp. 938–946, May 2013.

[8] J. Holtz and N. Oikonomou, "Optimal control of a dual three-level inverter system for medium-voltage drives," *IEEE Trans. Ind. Informat.*, vol. 46, no. 3, pp. 1034–1041, May 2010.

[9] B. A. Welchko, "A double-ended inverter system for the combined propulsion and energy management functions in hybrid vehicles with energy storage," in *Proc. 31st Annu. IEEE IECON*, 2005, pp. 1–6.

[10] M. Zhang, L. Hang, W. Yao, Z. Lu, and L. M. Tolbert, "A novel strategy for three-phase/switch/level (Vienna) rectifier under severe unbalanced grids," *IEEE Trans. Ind. Electron.*, vol. 60, no. 10, pp. 4243–4252, Oct. 2013.

[11] R. L. de Araujo Ribeiro, C. C. de Azevedo, and R. M. desouse, "A robust adaptive control strategy of active power filters for power factor correction, harmonic compensation, balancing of nonlinear loads," *IEEE Trans. Power Electron.*, vol. 27, no. 2, pp. 718–730, Feb. 2012.

[12] C. C. Hou and P. T. Cheng, "A multicarrier pulse width modulator for the auxiliary converter and the diode rectifier," *IEEE Trans. Power Electron.*, vol. 26, no. 4, pp. 1119–1126, Apr. 2011.

[13] S. Rahmani, N. Mendalek, and K. Al-Haddad, "Experimental design of a nonlinear control technique for three-phase shunt active power filter," *IEEE Trans. Ind. Electron.*, vol. 57, no. 10, pp. 3364–3375, Oct. 2010.

[14] K. Ma, M. Liserre, and F. Blaabjerg, "Operating and loading conditions of a three-level neutral-point-clamped wind power converter under various grid faults," *IEEE Trans. Ind. Appl.*, vol. 50, no. 1, pp. 520–530, Jan./Feb. 2014.

[15] B. A. Welchko and J. M. Nagashima, "A comparative evaluation of motor drive topologies for low-voltage, high-power EV/HEV propulsion systems," in *Proc. IEEE Symp. Ind. Electron.*, Jun. 2003, vol. 1, pp. 379–384.

[16] M. Kwak and S. K. Sul, "Control of an open-winding machine in a grid connected distributed generation system," *IEEE Trans. Ind. Appl.*, vol. 44, no. 4, pp. 1259–1267, Jul./Aug. 2008.

[17] M. Kwak and S. K. Sul, "Flux weakening control of an open winding machine with isolated dual inverters," in *Proc. IEEE Ind. Appl. Conf.*, Sep. 2007, pp. 251–255.

[18] E. Levi, I. N. W. Satiawan, N. Bodo, and M. Jones, "A space vector modulation scheme for multilevel open end winding five-phase drives," *IEEE Trans. Energy Convers.*, vol. 27, no. 1, pp. 1–10, Mar. 2012.

[19] T. Boller, J. Holtz, and A. K. Rathore, "Optimal pulsewidth modulation of a dual three-level inverter system operated from a single dc-link," *IEEE Trans. Ind. Appl.*, vol. 48, no. 5, pp. 1610–1615, Sep./Oct. 2012.

[20] V. T. Somasekhar, S. Srinivas, and K. K. Kumar, "Effect of zero vector placement in a dual-inverter fed open-end winding induction motor drive with alternate sub-hexagonal center PWM switching scheme," *IEEE Trans. Power. Electron.*, vol. 23, no. 3, pp. 1584–1591, May 2008.

[21] Y. Wang, D. Panda, T. Lipo, and D. Pan, "Open-Winding Power Conversion Systems Fed by Half-Controlled-Converters," *IEEE Trans. Power Electron.*, vol. 28, no. 5, pp. 2427–2436, May 2013.

[22] D. Pan and T. Lipo, "Series compensated open-winding PM generator wind generation system," in *Proc. 15th Int. Conf. EPE/EPMC*, 2012, pp. LS7c.1-1–LS7c.1-8.

[23] Y. Chou and H. Nian, "Sensorless control of PMSG based on dual two-level inverter open winding configuration for wind turbines," in *Proc. 15th ICEMS*, 2012, pp. 1–6.

[24] B. V. Reddy, V. T. Somasekhar, and Y. Kalyan, "Decoupled space-vector PWM strategies for a four-level asymmetrical open-end winding induction motor drive with waveform symmetries," *IEEE Trans. Ind. Electron.*, vol. 58, no. 11, pp. 5130–5141, Nov. 2011.

[25] S. D. G. Jayasinghe, D. M. Vilathgamuwa, and U. K. Madawala, "Direct integration of battery energy storage systems in distributed power generation," *IEEE Trans. Energy Convers.*, vol. 26, no. 2, pp. 677–685, Jun. 2011.

Heng Nian (M'09) received the B.Eng. and M.Eng. degrees from Hefei University of Technology, Hefei, China, in 1999 and 2002, respectively, and the Ph.D. degree from Zhejiang University, Hangzhou, China, in 2005, all in electrical engineering.

From 2005 to 2007, he was a Postdoctoral Fellow with the College of Electrical Engineering, Zhejiang University, where he has been an Associate Professor since 2007. His current research interests include optimal design and operation control for wind power generation systems.

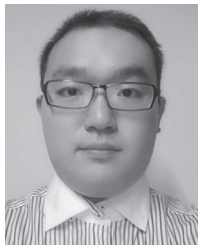

Yijie Zhou was born in Xiaogan, China, in 1990. He received the B.Sc. degree in electrical engineering from the College of Electrical Engineering, Zhejiang University, Hangzhou, China, in 2011, where he is currently working toward the Ph.D. degree.

His current research interests include motor control with power electronics devices in renewable-energy conversion, particularly the open winding permanent magnet synchronous generator systems with integration of multilevel converters.